Transient Stability Study of a Real-World Microgrid with 100% Renewables

Preprint

Yaswanth Nag Velaga,[1] Jing Wang,[1] Annabelle Pratt,[1] Laurence Abcede,[2] and Nagadev Shamukh[2]

1 National Renewable Energy Laboratory
2 San Diego Gas & Electric Company

Presented at the 2022 IEEE Energy Conversion Congress and Exhibition (ECCE)
Detroit, Michigan
October 9–13, 2022

NREL is a national laboratory of the U.S. Department of Energy
Office of Energy Efficiency & Renewable Energy
Operated by the Alliance for Sustainable Energy, LLC

This report is available at no cost from the National Renewable Energy Laboratory (NREL) at www.nrel.gov/publications.

Contract No. DE-AC36-08GO28308

Conference Paper
NREL/CP-5D00-82047
November 2022

Transient Stability Study of a Real-World Microgrid with 100% Renewables

Preprint

Yaswanth Nag Velaga,[1] Jing Wang,[1] Annabelle Pratt,[1] Laurence Abcede,[2] and Nagadev Shamukh[2]

1 National Renewable Energy Laboratory
2 San Diego Gas & Electric Company

Suggested Citation
Velaga, Yaswanth Nag, Jing Wang, Annabelle Pratt, Laurence Abcede, and Nagadev Shamukh. 2022. *Transient Stability Study of a Real-World Microgrid with 100% Renewables: Preprint*. Golden, CO: National Renewable Energy 82047. NREL/CP-5D00-82047. https://www.nrel.gov/docs/fy23osti/82047.pdf.

NREL is a national laboratory of the U.S. Department of Energy
Office of Energy Efficiency & Renewable Energy
Operated by the Alliance for Sustainable Energy, LLC

This report is available at no cost from the National Renewable Energy Laboratory (NREL) at www.nrel.gov/publications.

Contract No. DE-AC36-08GO28308

Conference Paper
NREL/CP-5D00-82047
November 2022

National Renewable Energy Laboratory
15013 Denver West Parkway
Golden, CO 80401
303-275-3000 • www.nrel.gov

NOTICE

This work was authored in part by the National Renewable Energy Laboratory, operated by Alliance for Sustainable Energy, LLC, for the U.S. Department of Energy (DOE) under Contract No. DE-AC36-08GO28308. Funding provided by U.S. Department of Energy Office of Energy Efficiency and Renewable Energy Solar Energy Technologies Office Agreement Number 9027. The views expressed herein do not necessarily represent the views of the DOE or the U.S. Government.

Cover Photos by Dennis Schroeder: (clockwise, left to right) NREL 51934, NREL 45897, NREL 42160, NREL 45891, NREL 48097, NREL 46526.

Transient Stability Study of a Real-World Microgrid with 100% Renewables

Yaswanth Nag Velaga
National Renewable Energy Laboratory
Golden, Colorado, USA
yaswanthnag.velaga@nrel.gov

Jing Wang
National Renewable Energy Laboratory
Golden, Colorado, USA
jing.wang@nrel.gov

Annabelle Pratt
National Renewable Energy Laboratory
Golden, Colorado, USA
annabelle.pratt@nrel.gov

Laurence Abcede
San Diego Gas & Electric Company
California, USA
labcede@sdge.com

Nagadev Shamukh
San Diego Gas & Electric Company
California, USA
nshanmukh@sdgecontractor.com

***Abstract*—This paper performs a transient stability study of a real-world microgrid that can operate with 100% renewables to better understand the stability and reliability of the microgrid under various dynamic scenarios. In particular, the operation of multiple grid-forming (GFM) and grid-following (GFL) inverters in such a power system is not well understood under dynamic operation conditions, such as islanding and black start; therefore, in this paper, an electromagnetic transient model of the microgrid is developed to investigate the stability of the system under various dynamic operating conditions and to identify potential reliability risks. The PSCAD/EMTDC simulation with the high-fidelity model provides helpful insights into the optimal operation modes of GFM and GFL inverters as well as the stability and reliability of the microgrid. It can also inform field deployment in terms of inverter control parameters and coordination as well as the expected performance of black start and unplanned islanding.**

***Index Terms*—Black start, droop control, grid-forming inverters, grid-following inverters, transient stability.**

I. Introduction

Higher levels of inverter-based resources (IBRs) in a microgrid reduce system inertia, which can cause voltage and frequency oscillations during dynamic conditions, leading to the degradation of microgrid stability and resilience [1]. Researchers have proposed inverters with virtual synchronous generator controls as a grid-forming (GFM) resource, but grid-following (GFL) inverters in microgrid stability studies are modeled as a single unit for simplicity [1]–[4]. If the units are aggregated, the potential interactions among multiple inverter units cannot be captured, as discussed in [5], [6]. From the literature, the transient stability of a microgrid with multiple GFM and GFL inverters is not well studied. In this paper, a high-fidelity electromagnetic (EMT) model of a real-world microgrid with 106 inverters (3 GFM and 103 GFL) is developed in PSCAD/EMTDC to study the interactions between them under dynamic events. Moreover, the inverter models in the literature are not equipped with ride-through and trip settings that comply with IEEE 1547-2018. In our PSCAD model, GFL inverter models are equipped with IEEE 1547-2018 ride-through and trip settings for our study even though many rooftop photovoltaic (PV) systems in the field are older and therefore not standard compliant.

The full-scale PSCAD simulation model is subjected to dynamic conditions, such as planned and unplanned islanding, to identify the potential stability and reliability risks. These studies will also be used to find the optimal modes of two GFM resources that can enhance network stability. Finally, black start of the microgrid using a GFM resource is simulated. The outcome of these studies on a real-world microgrid model will provide meaningful insights into microgrid stability and a good reference case study for field deployment and testing. The main contributions of the paper are to: 1) develop an accurate GFL PV inverter model reflecting field deployment with the correct control functions and IEEE 1547-2018 trip and ride-through settings; 2) study the optimal operation modes of the GFM inverters during various dynamic events to maintain system stability and reliability; 3) simulate various dynamic events to study the microgrid transient stability and reliability with multiple IBRs and understand the dynamic interactions between GFM and GFL inverters; and 4) provide key takeaways for field deployment based on the simulation of various dynamic events with the high-fidelity EMT model.

II. Descritpion of the Real-World Microgrid System

A. Borrego Springs Microgrid Model

The real-world microgrid is the Borrego Springs Microgrid, which is operated by San Diego Gas & Electric Company

This work was supported by Alliance for Sustainable Energy, LLC, the manager and operator of the National Renewable Energy Laboratory for the U.S. Department of Energy (DOE) under Contract No. DE-AC36-08GO28308. This material is based upon work supported by the U.S Department of Energy's Office of Energy Efficiency and Renewable Energy (EERE) under Solar Energy Technologies Office (SETO) Agreement Number 9027. The views expressed in the article do not necessarily represent the views of the DOE or the U.S. Government. The U.S. Government retains and the publisher, by accepting the article for publication, acknowledges that the U.S. Government retains a nonexclusive, paid-up, irrevocable, worldwide license to publish or reproduce the published form of this work, or allow others to do so, for U.S. Government purposes.

(SDG&E); several innovative microgrid technologies have previously been studied and demonstrated at this site [7]. The work presented in this paper is part of a project funded by the U.S. Department of Energy and led by SDG&E. The project goal is to demonstrate that a renewable energy microgrid can improve the resilience and stability of the electric system, perform black start without fossil fuel generators, and reduce PV curtailment by using GFM inverters and intelligent control of IBR assets. This will be shown through software simulations, as discussed in this paper, laboratory evaluations through hardware-in-the-loop simulation, and a field deployment.

The circuit topology of the microgrid is shown in Fig. 1. It consists of a 69-kV distribution substation; step-down transformers; three main circuits; and various IBRs, including a 26-MW PV facility (PV1), a 6.5-MW concentrating PV system (PV2), 5.4-MW of rooftop and distributed PV, two 1.8-MW diesel generators (Gen1 and Gen2), two utility-scale battery energy storage systems (SES1 and SES2) rated at 0.5-MVA/1.5-MWh and 1-MVA/3-MWh, respectively, and a 0.5-MVA/3-minute ultracapacitor energy storage system (SES3). SES1, SES2, and SES3 all have the same inverters, which are capable of operating in either GFM or GFL mode. Each circuit has three-phase dynamic loads, and Ckt1 and Ckt3 have pump loads with induction motors. The two diesel generators are not used in grid-connected mode, and they are backup generation in an islanded microgrid in case the GFM battery has a low state of charge (SOC). The main goal of the work described in this paper is to simulate the Borrego Springs Microgrid operating under 100% renewable resources and to evaluate the transient stability and reliability of the network. We performed a comprehensive EMT study to fully understand the stability and reliability of the Borrego Springs Microgrid under various dynamic scenarios. To this end, a high-fidelity model is developed to represent the microgrid system in the field: 1) The passive network without IBRs is manually developed based on an RSCAD model provided by SDG&E; and 2) 106 IBRs are modeled to reflect the field deployment (2 utility-scale battery systems, 1 ultracapacitor system, 20 PV units in the 26-MW PV facility, 1 concentrating PV unit of 6.5-MW, and 82 rooftop PV units (some units are aggregated)). For the test cases, 26-MW PV1 facility with 20 IBRs is not included. The IBRs include GFM and GFL inverters, which are described in the following subsections.

B. Grid-Forming Inverter

SES1, SES2, and SES3 are GFM inverters. The PSCAD model of the GFM inverter is developed to resemble the field device. The control diagram of the GFM inverter model is shown in Fig. 2. This GFM inverter model has a traditional double-loop structure with an outer loop for power control (PQ control) or voltage control (VF control), depending on the operational mode, and an inner current loop. There are three operation modes of the inverter model: startup (VF control), grid-connected (PQ control), and islanding master (VF control). The model shifts between the control modes based on the point of common coupling (PCC) circuit breaker

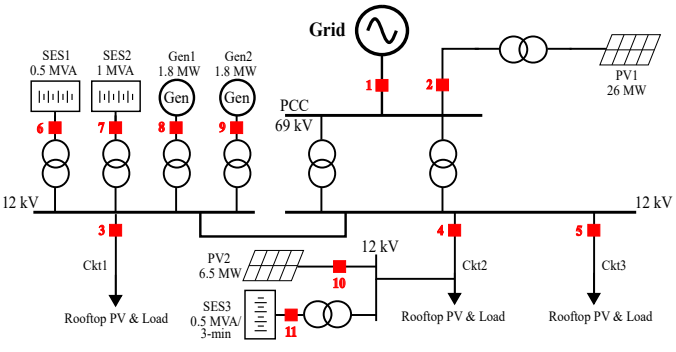

Fig. 1: Circuit topology of the Borrego Springs Microgrid.

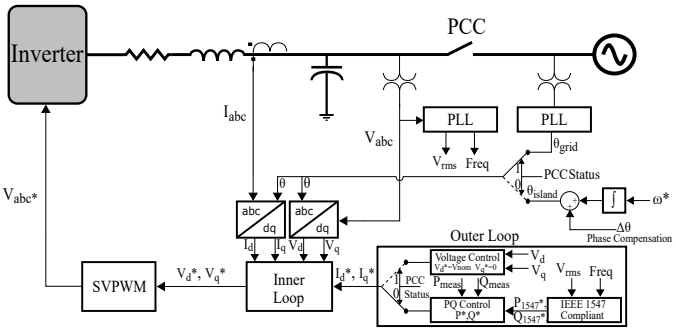

Fig. 2: GFM inverter control block diagram.

status. In PQ control mode, the GFM inverter is IEEE 1547-2018 compliant, as shown in Fig. 2.

The GFM inverter is initialized in VF control to start up and connect to the network by closing the PCC breaker after synchronization. When the PCC breaker is closed, the outer loop control shifts from VF to PQ mode following the power set points. In islanding master mode, ω is determined from the selected operation mode, i.e., isochronous mode or droop relationship. One important feature of this control structure is that the phase angle for the Park (abc/dq0) transformation switches between a grid-connected GFL angle (θ_{grid}) and an islanded self-generated angle (θ_{island}). To have a smooth islanding transition, the phase angle difference between the grid phase angle and the self-generated phase angle is calculated and added to the GFM inverter phase angle after the PCC circuit breaker is opened. The current references (I_d^*, I_q^*) generated from the outer loop are passed onto the inner current loop, which includes a feed-forward current loop. Finally, the voltage references from the inner current loop are converted to three-phase voltages through space vector pulse-width modulation, including DC-AC inverter dynamics.

The inverter model is also equipped with additional grid-supporting functions in GFL mode. These are discussed in the following subsections.

1) Active/Reactive Power Priority: Under normal operation, GFL inverters track the power reference commands subject to the maximum current limit. During frequency or voltage contingency events, inverters are required to support the grid by generating/absorbing active or reactive power; therefore,

the active (P) or reactive power (Q) reference command is implemented using current-limiting logic to prioritize one over the other. In an active power priority scenario, the model prioritizes the active power set point, and the reactive power is limited to the remaining device capacity. With reactive power priority, the model provides reactive power output in response to the voltage measurements at the terminal. The amount of power injection is determined from a predefined volt-var curve subject to the device rating. The reactive power output is changed once per second to minimize the oscillations. At the same time, the active power is curtailed if there is less capacity of active power than the commanded active power because of var priority. Note that SES3 uses a frequency fast response function to support and maintain the frequency during islanding operation.

2) Ride-Through Mode: During grid-connected mode, inverter tripping under grid disturbances can cause grid instability, leading to blackouts; therefore, interconnection standards require inverters to ride-through disturbances and restore power to the pre-disturbance levels [8]. During voltage disturbances, voltage sags at the inverter terminals trigger voltage ride-through mode. For voltages outside the continuous operating range, the model stays connected in constant power mode or enters cessation mode. During frequency disturbances, the model responds by increasing/decreasing the active power based on a droop relationship. The magnitude of the active power is calculated from the equations described in Table 23 of IEEE 1547-2018 interconnection standard.

C. Grid-Following Inverter

PV1, PV2, and the rooftop PV are modeled as GFL inverters. All GFL inverters are average models of a controlled voltage source followed by a filter. The control block diagram is shown in Fig. 3. The PV1 model can work in either PQ control mode or with a smart inverter function (volt-var with var priority and active power maximum power point tracking). The PV1 model has an LCL filter, with the parameters obtained from the field. PV2 is an old and noncontrollable facility, and it works in unity power factor mode. The distributed rooftop PV units operate in unity power factor. PV2 and the rooftop PV are modeled using an L filter. PV1 is IEEE 1547-2018 compliant in the field, and the rooftop PV units are IEEE 1547-2003 compliant; thus, the voltage and frequency trip and ride-through settings are included in the PSCAD model. Note that the 26-MW PV facility, PV1, consists of 54 inverters of 500-kW each in the field, but it is aggregated and modeled using 20 inverters of 1.3-MW each in PSCAD. The 6.5-MW of rooftop PV are distributed in the field, but the rooftop PV is aggregated and modeled using 82 inverters of different ratings and locations based on the data from the field.

III. TESTING OBJECTIVES AND PERFORMANCE METRICS

The objective of the Borrego Springs project is to run the microgrid using 100% renewable energy sources and to evaluate the transient stability and reliability of the microgrid

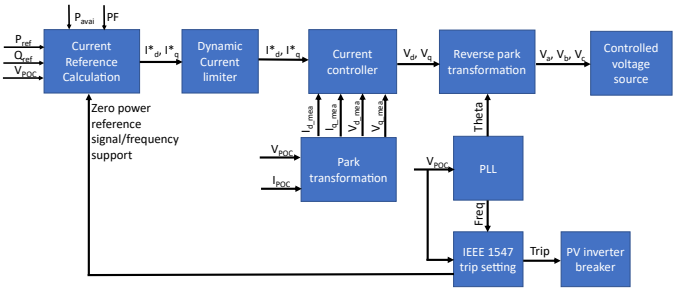

Fig. 3: GFL inverter control block diagram.

TABLE I: Performance Metrics of the Microgrid Under Dynamic Events

	Voltage	Frequency
Transient	ΔV_{max}, dv/dt, settling time	Δf_{max}(nadir), df/dt, settling time
Steady state	V, ΔV, standard deviation	f, Δf, standard deviation

in a low-inertia environment. To evaluate the stability of the microgrid through the EMT simulation, the microgrid model needs to be tested under various dynamic conditions. The main objectives of the testing are to:

- Analyze the performance of the GFM inverter model in GFM, GFL, and black-start modes to identify the appropriate control parameters/settings in each operating mode.
- Find suitable operating modes for SES1, SES2, and SES3 (e.g., VF control, PQ control, grid support) under various dynamic events.
- Identify the interactions between the GFM and GFL inverters during dynamic events.
- Demonstrate the transient stability of the microgrid under transient conditions, including solutions to solve potential problems during the testing.

Results in each test scenario are evaluated through the performance metrics defined in Table I. These metrics will be used to fine-tune the control parameters and settings of the GFM and GFL inverters to improve the transient dynamics of the microgrid.

IV. TEST CASES AND RESULTS

To simulate multiple IBRs (86), the high-fidelity passive network developed in PSCAD is split into three networks using the Bergeron cable model. Bergeron model is based on distributed LC parameter line model. The first network contains the transmission grid and the microgrid yard IBR assets, Ckt1 and PV1; the second network contains Ckt2; and the third contains Ckt3. PV1, PV2, and the rooftop PV are modeled as GFL inverters. The line length of two Bergeron cables is kept at 1 km because longer lines generate additional reactive power. Based on the traveling wave time estimation using $\sqrt{LC}$, the maximum simulation time step is determined from the Bergeron cable line lengths. For all the test cases, the simulation time step is 25 μs. The utility-scale battery storage devices (SES1 and SES2) in Fig. 1 are modeled as GFM

inverters using the control structure shown in Fig. 2. In grid-connected mode, SES1 and SES2 stay connected to the system with zero power reference input and can respond to disturbances if required. Due to its larger battery capacity, SES2 is always the islanding master for islanding operation, providing the voltage and frequency reference to the microgrid. SES1 primarily operates as a GFL device in planned/unplanned islanding scenarios; however, one objective of the study is to determine the SES1 optimal operation mode (GFL/GFM) in an islanded configuration to improve the microgrid transient stability. The ultracapacitor energy storage system (SES3) has the same GFM-capable inverter but is only operated in GFL mode with a fast frequency response. SES3 is designed to discharge full power in 3 minutes, providing fast frequency support during the islanding transition. Note that this paper focuses on light loading scenarios, and therefore the PV1 facility is not included in the simulation. In future studies, the PV1 facility will be used for high loading scenarios.

To verify the performance of a 100% renewable microgrid with 86 IBRs, different test scenarios are simulated in PSCAD, including unplanned islanding and black-start events. Each test scenario is based on the load and solar insolation profiles shown in [9]. In this article, load and solar conditions at 10:00 AM are assumed for the studies. Based on the solar insolation data, the PV systems generate at 60% of installed capacity. The main objective of these test scenarios is to study the performance of the GFM inverter model with almost 86 IBRs. The optimal control mode for SES1 can also be studied using the three unplanned islanding test scenarios. A black-start scenario is also simulated.

A. Scenario 1: Unplanned Islanding with SES2 as GFM Source and SES1 in GFL Mode

The purpose of this test scenario is to study the performance of a 100% renewable microgrid during unplanned islanding with SES2 as a single GFM source. In this scenario, SES2 is configured to operate in VF control mode (isochronous), and SES1 is configured in PQ control mode. The ultracapacitor device (SES3) stays connected to provide fast frequency support during the transition. The SOC of the SES1 and SES2 devices are assumed to be at 80%. The SOC is not monitored because the duration of the simulation is 10 s. The PV2 facility is either connected or disconnected because it is not dispatchable. In this scenario, it is assumed to be connected, and it generates power at 60% of installed capacity. To supply the reactive power, two capacitor banks of 1.2 MVAR each in Ckt1 and Ckt3 are connected in grid-connected and islanded modes; therefore, SES1, SES2, SES3, PV2, the rooftop PV, and two capacitor banks are the power generation sources in the islanded microgrid. Based on the load profile, there is surplus active power available, which means that the GFM source will need to absorb the excess power subject to their device ratings. This is particularly important for transient stability during transitions, which is discussed in Section IV-E.

SES2 starts at t = 0 s as a GFM source and establishes the voltage and frequency as the grid-connected networks ramps up. At t = 2 s, a synchronization enable signal is sent to SES2. The voltage, frequency, and phase angle are actively changed to bring the difference between the grid and SES2 to within the predefined limits. BKR 7 in Fig. 1 is closed using a synchronization relay monitoring the voltage, frequency, and phase difference parameters. When BKR 7 is closed, SES2 changes to GFL mode with zero power reference. At t = 5.6 s, the microgrid PCC circuit, BKR 1, is opened to create and unplanned islanding scenario.

The results of the unplanned islanding scenario at t = 5.6 s are shown in Fig. 4. Instantaneous voltages at the PCC and SES2 show the smooth transition from the grid-connected to islanding scenario. The SES2 frequency shows the damped oscillation settling back at 60 Hz because of the isochronous mode. The microgrid frequency, measured at the PCC, overshoots by 0.2 Hz and dampens within 3 s after the grid separation. The active and reactive power measurements of SES2 show the small damped oscillations settling at 2 s, which indicates the stability of the microgrid with SES2 as a single GFM source. SES1 operating in GFL mode continues to inject active and reactive power (Fig. 4) before and after the islanding operation. Since the frequency of the microgrid is within the bandwidth, SES3 is not required to inject power during the transition and therefore the power measurements are not shown. All the results in scenario 1 show that the unplanned islanding is successful.

B. Scenario 2: Unplanned Islanding with SES1 and SES2 as GFM Sources in Isochronous Mode

In this scenario, both SES1 and 2 battery storage devices are operating as GFM sources. The purpose of this test scenario is to evaluate the performance of two GFM sources located in proximity and to evaluate the transient stability of the grid during the transition. All the assumptions discussed in scenario 1 are applicable here except for the SES1 operation mode.

SES1 and SES2 start at t = 0 s as GFM sources and establish the voltage and frequency at their terminals. At t = 2 s and 2.2 s, synchronization enable signals are sent to SES2 and SES1, respectively. As the active synchronization control block changes the SES1 and SES2 voltage, frequency, and phase angle parameters, the synchronization relay connected across the breakers monitors the parameters and closes the breaker after they fall under predefined limits. SES1 and SES2 operate in GFL mode with zero power reference commands. At t = 5.6 s, the 69-kV microgrid PCC BKR 1 is opened to create an unplanned islanding scenario.

The voltage results of PCC, SES2, and SES1 in Fig. 5 show a smooth transition, as in scenario 1. The SES1 and SES2 frequency show a maximum overshoot of 0.15 Hz. The settling time for the damped frequency oscillations is 1.5 s. Even the power measurements in Figs. 5 & 6 show the settling time of 1.5 s. The SES2 terminal voltage rises to 1.03 p.u. against the 1.0 p.u. reference voltage because of excess reactive power in the microgrid. SES3 is not required to inject any power because the frequency is within the deadband limit of SES3. A comparison to scenario 1 shows that two GFM resources

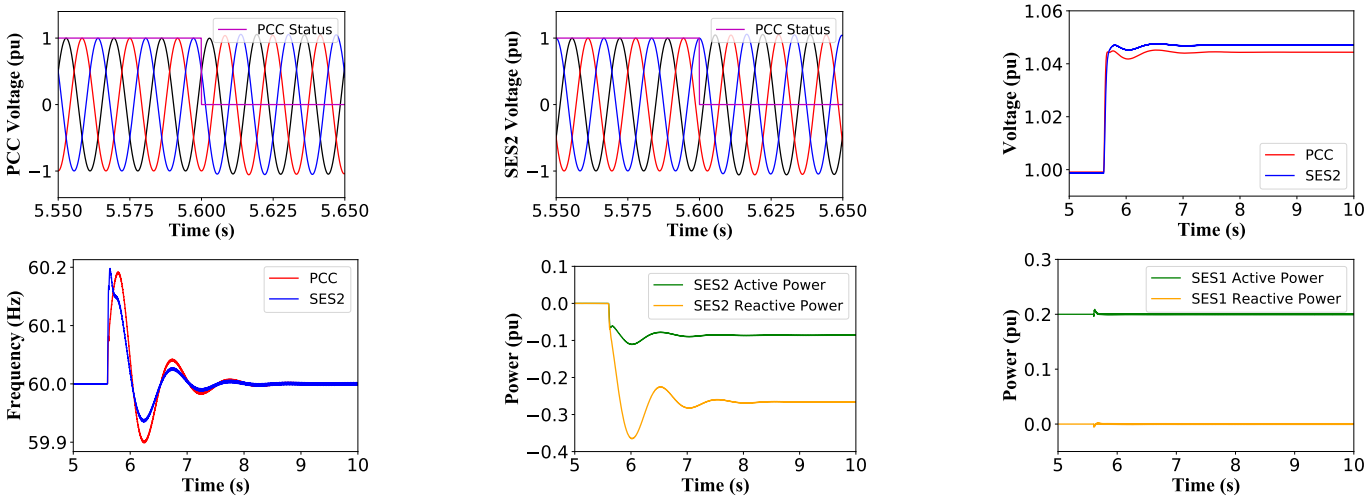

Fig. 4: Scenario 1: PCC and SES2 voltage waveforms and root mean square (RMS) voltages, frequency, and SES2, SES1 power measurements.

provide a better transient response than one GFM resource in the Borrego Springs Microgrid.

C. Scenario 3: Unplanned Islanding with SES1 and SES2 as GFM Sources in Droop Mode

This test scenario is similar to scenario 2 except both SES1 and SES2 are operating in droop mode. The purpose of this scenario is to evaluate the performance of two GFM sources in droop mode. The results will show the effect of droop mode on transient stability. The startup sequence is the same as the procedure described in scenario 2. The droop constants of SES1 and SES2 are set to 4%. When there is more than one generation source in the network, droop mode is preferred over isochronous mode. Droop mode with IBRs exhibits stability issues during transition phases. The outer loop in GFM mode is changed to proportional derivative (PD) control to provide a stable response.

The results from scenario 3 in Fig. 7 show that the behavior of the GFM inverter is similar to that in scenario 2. Due to the droop mode and surplus generation, the frequency settles above 60 Hz. The settling time of the oscillations in the power measurements (Figs. 7 & 8) is similar to the measurements in scenario 2. To determine the better operating mode between isochronous and droop control, more challenging scenarios, including load steps and generation loss, are required.

D. Scenario 4: Black Start of Borrego Microgrid Circuit 1

In this scenario, the microgrid system is blacked out, and the PCC circuit breaker is open to test the black-start capability of SES2. The objective is to use SES2 as a GFM source and SES1 as a GFL source to fully energize Ckt1, which includes rooftop PV, so the diesel generators are offline for these simulations. Ckt1 has a radial structure, as shown in Fig. 9, which includes three zones that were identified based on the switching sequence. Zone 1 has light, balanced load and rooftop PV, and zones 2 and 3 both have heavy unbalanced load and rooftop PV. In PSCAD, each Ckt1 load in Fig. 9 is modeled as constant power (CP) and constant impedance (CI). The circuit load data and rooftop PV installed PV capacity are shown in Fig. 9. Note that the breakers are numbered in the sequence they operate.

The load and rooftop PV insolation conditions for Ckt1 are assumed to be the same as in scenarios 1, 2, and 3. The accelerated black-start sequence is performed as follows: 1) SES2: Start the simulation and enable SES2 in startup (VF control) mode so that it can serve as a black-start GFM source; SES2 ramps up and energizes the 480-V bus; BKR 1 closes at 1.5 s to connect with the grid connection transformer and energize the 12-kV bus. 2) SES1: With the 12-kV bus energization, BKR 2 closes at 2.5 s to connect SES1 in PQ control mode; SES2 works as a standby, with zero power generation. 3) Zone 1: Close BKR 3 to energize the N102 and N103 nodes at 4 s, and all four loads (2 CP and 2 CI) are connected at the same time; the rooftop PV comes online at 12 s with an 8 s delay after the N103 energization; the rooftop PV starts with zero power output, and it ramps up to 60% capacity based on assumed solar insolation conditions with 0.95 lagging power factor. 4) Close BKR 4 at 15 s, energizing the N104 and N107 nodes. 5) Zone 2: Close BKR 5 and BKR 6 at 17 s and 25 s, respectively, to energize the Zone 2 nodes. 7) To reduce the power output from SES2, increase the SES1 contribution by changing the power reference commands at 27 s to 0.8 p.u. and 0.95 lagging power factor. 8) Before PV2 comes online, switch the capacitor bank in Zone 2 at 29 s to contribute 1.2-MVAR reactive power for voltage stability. 9) The larger PV (PV2) in Zone 2 comes online at 33 s with 60% generation and 0.95 power factor operation; 10) Zone 3: Connect the N108 load by closing BKR 8 at 40 s, and connected the aggregated rooftop PV to the circuit at 48 s. 11) Connect the final load in the circuit by closing BKR 9 at 55 s; subsequently, the rooftop PV at N109 generates 60%

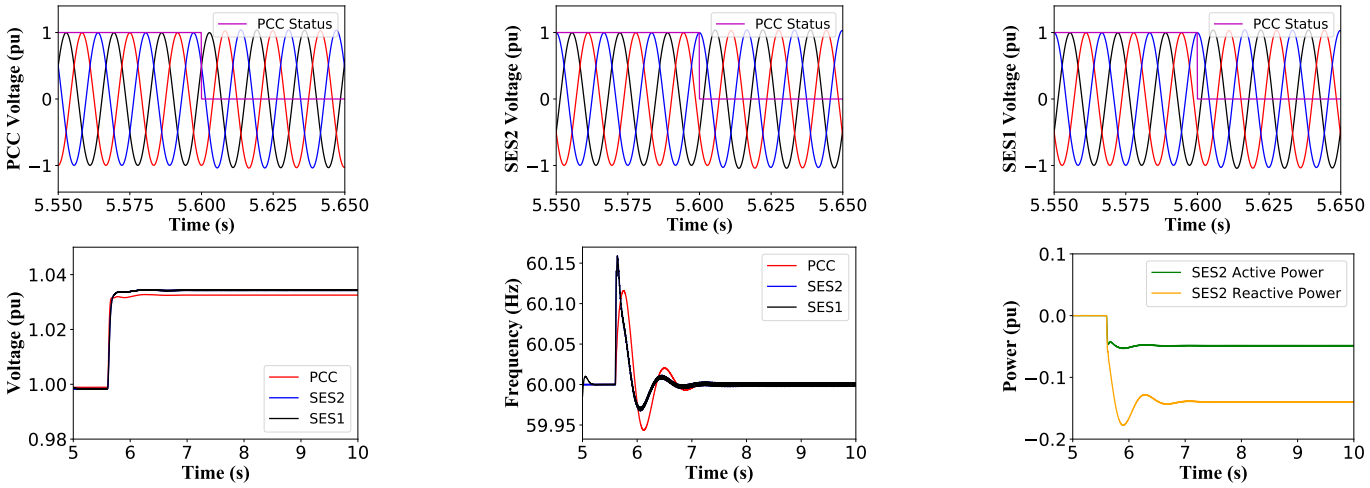

Fig. 5: Scenario 2: PCC, SES2, and SES1 voltage, frequency, and power measurements.

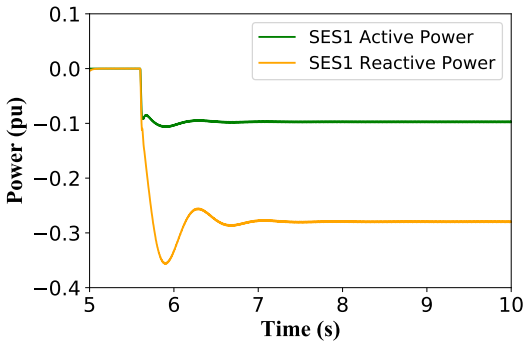

Fig. 6: Scenario 2: SES1 power measurements.

capacity from 63 s.

Figure. 10 shows the voltage, frequency, and active and reactive power measurements of the primary side of the transformer that connects to the SES2. The voltage and frequency measurements show that the overall black-start process is successful. These measurements show noise from 27 s with the addition of the zone 2 and 3 unbalanced load. This load causes negative-sequence harmonics, but the positive-sequence dq0 control in the SES2 inverter can only control the fundamental frequency component. A notch filter tuned to suppress the second harmonic is applied to the dq voltage measurements to filter out the second harmonic caused by the negative-sequence component. Due to the presence of third and fourth harmonics, the measurements become more noisy with each addition of unbalanced load.

During the black-start process, the voltage and frequency are maintained at 1 p.u. and 60 Hz, respectively. The transient spikes shown in Fig. 10 are due to the connection of the capacitor banks and the rooftop PV. In particular, the connection of a capacitor bank at 29 s causes a big transient spike in frequency and is also reflected in the voltage measurements. The connection of the end-of-line PV at N106 with a large capacity of 700-kW causes another spike in voltage and frequency (at 33 s). Most transients in the voltage and frequency measurements are caused by the addition of the rooftop PV units, which indicates interactions between the GFM and GFL inverters. Remember that PV2, PV3, and PV4 have four GFL units connected in parallel. The active power output of SES2 shows a more expected response, increasing power with load connected and decreasing power with PV connected. The reactive power output shows a big transition from supplying reactive power to absorbing at 29 s because of the 1.2-MVAr capacitor bank switching.

Figure. 10 also shows the voltage and power measurements at N106. The node is energized at 27 s, and the voltage ramps up to 0.98 p.u. until the capacitor bank switching. Due to the reactive power from the capacitor bank, the voltage at N106 is maintained between 1 p.u. and 1.02 p.u. The active power demand at N106 increases to 650-kW at 29 s but decreases to near zero because of large rooftop PV coming online at 33 s. Overall, the results presented in Fig. 10 indicate a successful fast black start of Ckt1.

E. Summary of Simulation Results and Discussion

1) Unplanned Islanding: Three scenarios are simulated for the unplanned islanding operation with single/multiple GFM inverters operating in isochronous or droop mode. SES1, SES2, SES3, PV2, rooftop PV, and two capacitor banks are the power generation sources in the islanded microgrid. Based on the selected load conditions, local generation is greater than the microgrid load in grid-connected and islanded modes. The key results of the unplanned islanding scenario are:

- The results of all scenarios show a smooth transition from grid-connected to islanded mode thanks to the extensive tuning of the GFM inverter control parameters.
- In scenario 1, with a single GFM source, the frequency and power measurements show oscillatory behavior before reaching steady state. This response can be further improved with tuning the damping time constant.

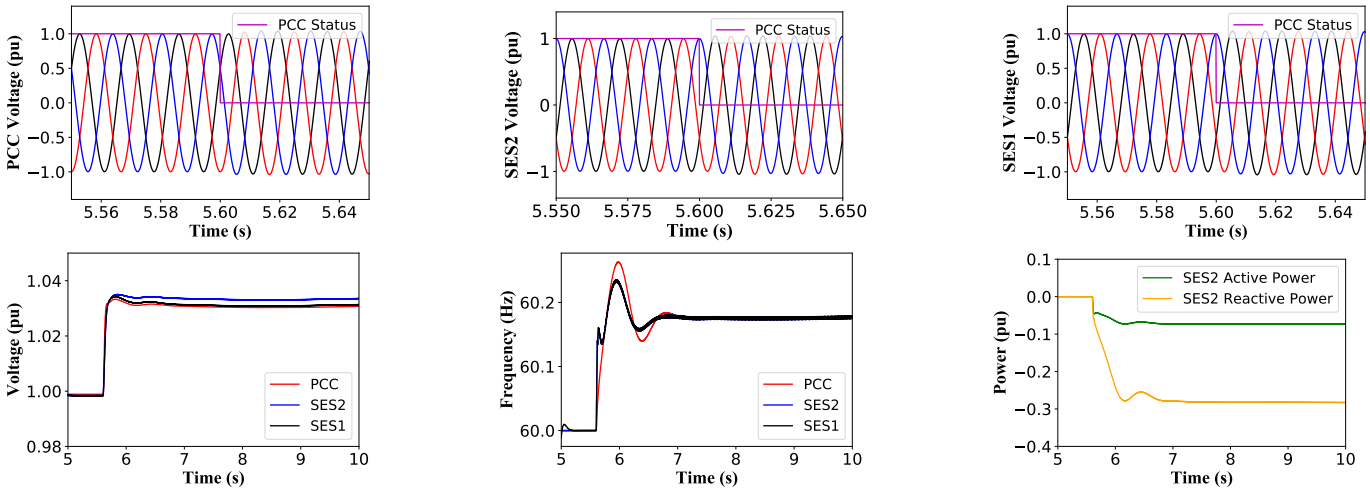

Fig. 7: Scenario 3: PCC, SES2, and SES1 voltage, frequency, and power measurements.

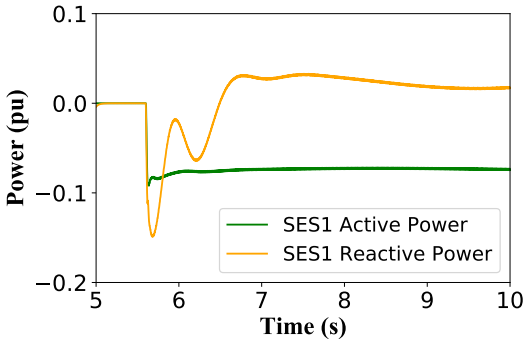

Fig. 8: Scenario 3: SES1 power measurements.

- By comparing all three scenarios, two GFM sources show a better transient response than a single GFM source, and similar transient responses (overshoot and settling times) are observed with two GFM sources.
- Droop control allows two GFM inverters to share the active and reactive power, which will not saturate the GFM inverter like the isochronous mode does. To choose between isochronous and droop mode, more challenging testing scenarios are required.

Achieving a stable response in unplanned islanding scenarios required extensive tuning of the GFM control parameters (proportional integral (PI) control of voltage and current loop). The key learnings from tuning the GFM inverter controls are summarized as follows:

- In the case of overgeneration, the GFM inverter needs to absorb power. Its transient response is unstable with outer voltage loop PI control. The tuning of the PI control parameters could not solve the oscillation problem.
- Proportional integral derivative (PID) control is used and has a stable response because D-control provides a damping effect. But the settling time is longer than the ones without D-control.

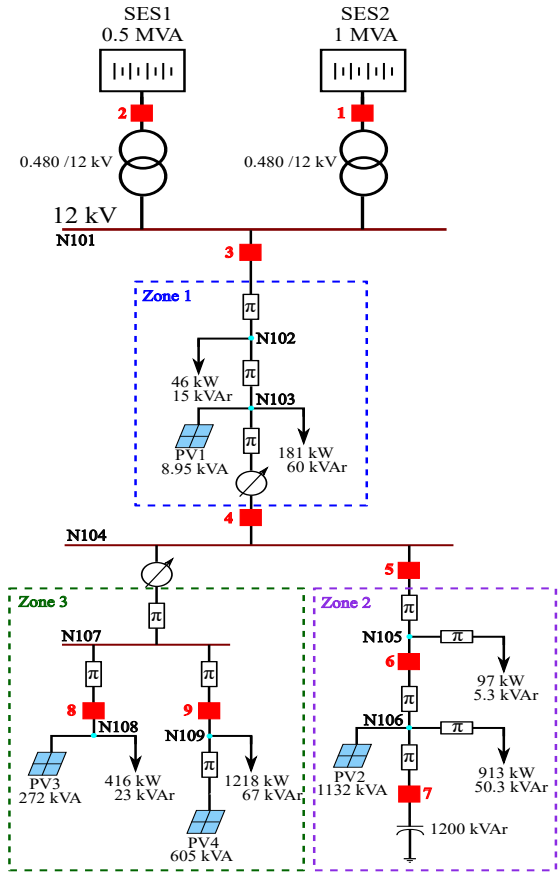

Fig. 9: Circuit one-line diagram for black start.

- PD control shows a better response than PID control, especially in scenario 3 (two GFM inverters in droop mode) because there is no tracking error accumulated with I-control to saturate the inner current loop.

From the three scenario results, SES1 operating in VF control mode requires adjusting its control parameters because

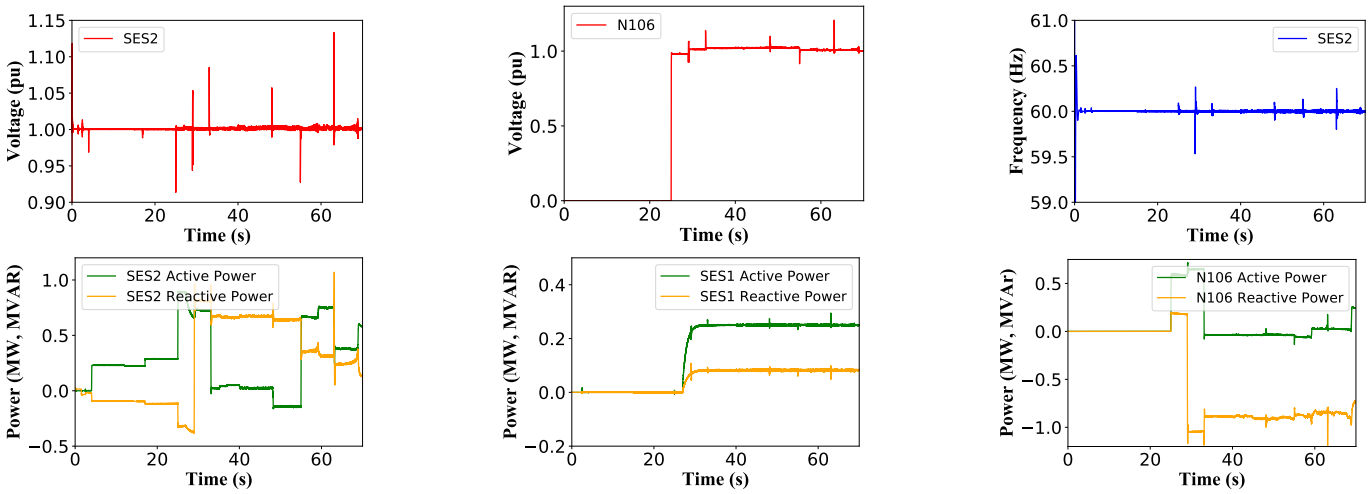

Fig. 10: Scenario 4: SES2, and N106 end-of-line voltage, frequency, and power measurements.

SES1 and SES2 are connected to the same 12-kV bus and the interactions between the two GFM inverters are direct and undamped. When SES1 is operating in PQ control mode, only the SES2 inverter controls needs to be tuned— compared to having to tune both the SES1 and SES2 parameters for scenarios 2 and 3. To validate the SES1 operation mode, more challenging test scenarios are required.

2) Black Start: The results presented in Figs. 9 and 10 show the successful black start of the Borrego Springs Microgrid using 100% renewable energy. Achieving the successful black start with renewable resources requires the proper sequence of load switching and active and reactive power generation balancing to avoid saturating the GFM source. A few challenges were encountered during the black-start simulations. The main challenge is with the presence of unbalanced load in the microgrid. The GFM inverter in dq0 control only performs well if there are only fundamental components. With unbalanced load, there exist negative-sequence components in the system, which affects the stability and performance of the GFM inverter. A notch filter is used in this work to suppress the second harmonic caused by the unbalanced load and to reduce the noise in the dq0 components. Figs. 9 and 10 show some noise due to the unsuppressed harmonics. To further reduce the noise, negative-sequence control or harmonic compensation control is required.

Conclusion

This paper presents the transient stability study of a real-world microgrid operating with 100% renewable energy sources. The transient response of a microgrid with 3 GFM and almost 83 GFL devices is tested through three unplanned islanding scenarios and a black-start event. Results from all three scenarios showed that the transition is smooth from grid-connected to islanded mode. Unplanned islanding with two GFM inverters has a better transient response in terms of overshoot and settling time. Two GFM inverters operating in isochronous and droop mode showed similar behavior, but droop mode requires tuning the control parameters. The black start of one circuit in the microgrid was successful. More test scenarios will be simulated to test the islanded microgrid transient stability in future studies. The main importance of these studies is to use the high-fidelity model to run EMT simulations and to assist in the field operation and deployment to achieve expected responses. These studies also highlight the role of GFM inverter controls and operating modes on microgrid stability with 100% renewable resources.

Acknowledgments

Authors would like to thank Farhad Elyasi from Quanta Technology for providing the RSCAD GFM inverter model.

References

[1] T. Kerdphol, M. Watanabe, K. Hongesombut, and Y. Mitani, "Self-Adaptive Virtual Inertia Control-Based Fuzzy Logic to Improve Frequency Stability of Microgrid With High Renewable Penetration," *IEEE Access*, vol. 7, pp. 76071–76083, 2019.

[2] C. Yuan, P. Xie, D. Yang, and X. Xiao, "Transient Stability Analysis of Islanded AC Microgrids with a Significant Share of Virtual Synchronous Generators," *Energies*, vol. 11, p. 44, Jan. 2018.

[3] X. Huang, K. Wang, J. Qiu, L. Hang, G. Li, and X. Wang, "Decentralized Control of Multi-Parallel Grid-Forming DGs in Islanded Microgrids for Enhanced Transient Performance," *IEEE Access*, vol. 7, pp. 17958–17968, 2019.

[4] U. Markovic, O. Stanojev, E. Vrettos, P. Aristidou, and G. Hug, "Understanding Stability of Low-Inertia Systems," preprint, engrXiv, Feb. 2019.

[5] F. Cavazzana, T. Caldognetto, P. Mattavelli, M. Corradin, and I. Toigo, "Analysis of Current Control Interaction of Multiple Parallel Grid-Connected Inverters," *IEEE Transactions on Sustainable Energy*, vol. 9, pp. 1740–1749, Oct. 2018.

[6] T. Orchi, M. Mahmud, and A. Oo, "Generalized Dynamical Modeling of Multiple Photovoltaic Units in a Grid-Connected System for Analyzing Dynamic Interactions," *Energies*, vol. 11, p. 296, Jan. 2018.

[7] Hilal Katmale, Sean Clark, Thomas Bialek, and Laurence Abcede, "Borrego Springs: California's First Renewable Energy- Based Community Microgrid," Tech. Rep. CEC-500-2019-013, Feb. 2019.

[8] "IEEE Standard for Interconnection and Interoperability of Distributed Energy Resources with Associated Electric Power Systems Interfaces," tech. rep., IEEE.

[9] J. Wang, A. Pratt, K. Prabakar, B. Miller, and M. Symko-Davies, "Development of an integrated platform for hardware-in-the-loop evaluation of microgrids prior to site commissioning," *Applied Energy*, vol. 290, p. 116755, May 2021.